Comput Mech (2015) 55:1131–1141
DOI 10.1007/s00466-014-1095-0

ORIGINAL PAPER

Space–time computational analysis of MAV flapping-wing aerodynamics with wing clapping

Kenji Takizawa · Tayfun E. Tezduyar · Austin Buscher

Received: 19 October 2014 / Accepted: 28 October 2014 / Published online: 6 January 2015

Abstract Computational analysis of flapping-wing aerodynamics with wing clapping was one of the classes of computations targeted in introducing the space–time (ST) interface-tracking method with topology change (ST-TC). The ST-TC method is a new version of the deforming-spatial-domain/stabilized ST (DSD/SST) method, enhanced with a master–slave system that maintains the connectivity of the "parent" fluid mechanics mesh when there is contact between the moving interfaces. With that enhancement and because of its ST nature, the ST-TC method can deal with an actual contact between solid surfaces in flow problems with moving interfaces. It accomplishes that while still possessing the desirable features of interface-tracking (moving-mesh) methods, such as better resolution of the boundary layers. Earlier versions of the DSD/SST method, with effective mesh update, were already able to handle moving-interface problems when the solid surfaces are in near contact or create near TC. Flapping-wing aerodynamics of an actual locust, with the forewings and hindwings crossing each other very close and creating near TC, is an example of successfully computed problems. Flapping-wing aerodynamics of a micro aerial vehicle (MAV) with the wings of an actual locust is another example. Here we show how the ST-TC method enables 3D computational analysis of flapping-wing aerodynamics of an MAV with wing clapping. In the analysis, the wings are brought into an actual contact when they clap. We present results for a model dragonfly MAV.

Keywords Flapping-wing aerodynamics · Wing clapping · MAV · Contact · Topology change · Space–time interface-tracking

K. Takizawa (✉)
Department of Modern Mechanical Engineering and Waseda Institute for Advanced Study, Waseda University, 1-6-1 Nishi-Waseda, Shinjuku-ku, Tokyo 169-8050, Japan
e-mail: kenji.takizawa@tafsm.org

T. E. Tezduyar · A. Buscher
Mechanical Engineering, Rice University – MS 321, 6100 Main Street, Houston, TX 77005, USA
e-mail: tezduyar@tafsm.org

1 Introduction

Lift-generation outcome of wing clapping has been substantiated both experimentally [1] and theoretically [2]. The mechanism has been used in laboratory MAVs to increase the lift- and thrust-generation efficiency (see, for example, [3]). Computational analysis of flapping-wing aerodynamics with wing clapping requires the accuracy of interface-tracking (moving-mesh) methods, flexibility of being able to deal with the topology change (TC) in the fluid mechanics mesh when the wings are brought into contact, and the computational practicality of accomplishing these in 3D analysis. The space–time (ST) interface-tracking method with TC (ST-TC), introduced in [4], satisfies these requirements. The ST-TC method is a new version of the deforming-spatial-domain/stabilized ST (DSD/SST) method. The DSD/SST method was introduced in [5–7] as a core computational technology for flow problems with moving boundaries and interfaces and since then has been gaining more and more power [8–12]. Its moving-mesh feature makes it comparable to the Arbitrary Lagrangian–Eulerian (ALE) formulation [13], which is the most widely used moving-mesh method, with many successful applications in fluid–structure interaction (FSI) (see, for example, [12,14–52]).

Computations based on the DSD/SST method also have been very successful in a number of classes of fluid mechanics and FSI problems, and formidable computational challenges were addressed with the special methods targeting those classes of problems. Examples, with the cited references reporting recent computations, are spacecraft aerodynamics [53], spacecraft parachutes [12,54–60], cardiovascular fluid mechanics [4,60–67], flapping-wing aerodynamics [4,60,64,68–70], wind-turbine aerodynamics [60,64,71,72], and data compression [73].

Both the ALE and DSD/SST methods possess the desirable features of moving-mesh methods, including mass conservation across the interface and better resolution of the boundary layers. The boundary layers are resolved more accurately because as the fluid–solid interface moves, the refined-mesh region follows the interface. These desirable features do not come easily or do not come at all with the interface-capturing (nonmoving-mesh) methods. Comments on and examples for what the DSD/SST method brings to the table beyond what the ALE method does can be found in [4], and also in [4,10–12,60,64,66,68–73], including examples from aerodynamics of flapping wings and wind turbines and fluid mechanics of heart valves.

In its ST-TC version, the DSD/SST method is enhanced with a master–slave system that maintains the connectivity of the "parent" fluid mechanics mesh when there is contact between the moving interfaces. With that enhancement and because of its ST nature, the ST-TC method can deal with an actual contact between solid surfaces in flow problems with moving interfaces. It accomplishes that while still possessing the desirable features of moving-mesh methods, the key desirable feature being better resolution of the boundary layers.

Even before its ST-TC version, the DSD/SST method, with effective mesh update, was already able to handle moving-interface problems when the solid surfaces are in near contact or create near TC. Flapping-wing aerodynamics of an actual locust [12,60,64,68], with the forewings and hindwings crossing each other very close and creating near TC, is an example of successfully computed problems. Flapping-wing aerodynamics of a micro aerial vehicle (MAV) with the wings of an actual locust [60,64,69,70] is another example. However, as commented in [4], in some moving-interface problems with contact between the solid surfaces, the "nearness" that can be modeled with a moving-mesh method without actually bringing the surfaces into contact might not be "near" enough for the purpose of solving the problem. It was mentioned in [4] that fluid–solid interface-tracking/interface-capturing technique (FSITICT) [74] was motivated by such FSI problems.

In the FSITICT, we track the interfaces wherever and whenever we can with a moving mesh, and capture over that moving mesh the interfaces we cannot track, specifically the interfaces where and when we need to have an actual contact between the solid surfaces. As commented in [66], essentially, the FSITICT is based on giving up on the

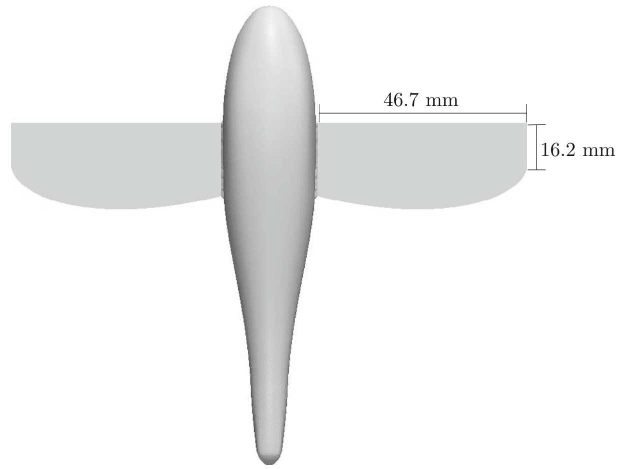

Fig. 1 Wing dimensions

interface-tracking accuracy in the parts of the domain where and when we expect an actual contact. As also commented in [66], while this is better than giving up on the interface-tracking accuracy everywhere in the domain by using purely an interface-capturing method, the flow would not be represented accurately between the solid surfaces as they close.

The ST-TC method does not give up on interface-tracking accuracy even where there is an actual contact between solid surfaces or other TC. It does not require unstructured ST mesh generation. Details of the ST-TC method can be found in [4], together with conceptual examples and 2D test computations with models representative of the classes of problems targeted with the method. In [66], the ST-TC method was extended to 3D fluid mechanics computation of an aortic valve with coronary arteries and a mechanical aortic valve. Here we show how the ST-TC method enables 3D computational analysis of flapping-wing aerodynamics of an MAV with wing clapping. We use a model dragonfly MAV as the test problem. In the analysis, the wings are brought into an actual contact when they clap. The computational analysis is presented in Sect. 2, and the concluding remarks are given Sect. 3.

2 Dragonfly MAV

2.1 Geometry and flapping-motion modeling

The design of the wings is similar to the design in a toy MAV [75], and the body is the same as the MAV body in [69]. The span of the single wing is 46.7 mm, and the minimum, maximum and average chord lengths are 16.2, 19.2 and 17.6 mm, respectively (see Fig. 1). The wings have zero thickness and undergo prescribed flapping, as shown in Figs. 2 and 3, with a period of $T = 0.0365$ s. Figure 4 shows the contact point

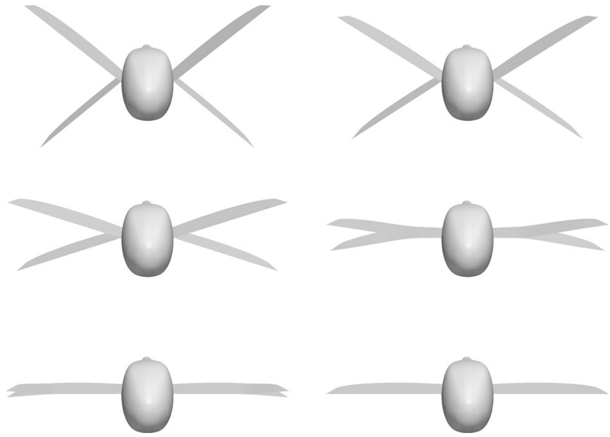

Fig. 2 Wing configurations at $t/T = 0.0, 0.1, 0.2, 0.3, 0.4$ and 0.5 (*left* to *right* and then *top* to *bottom*)

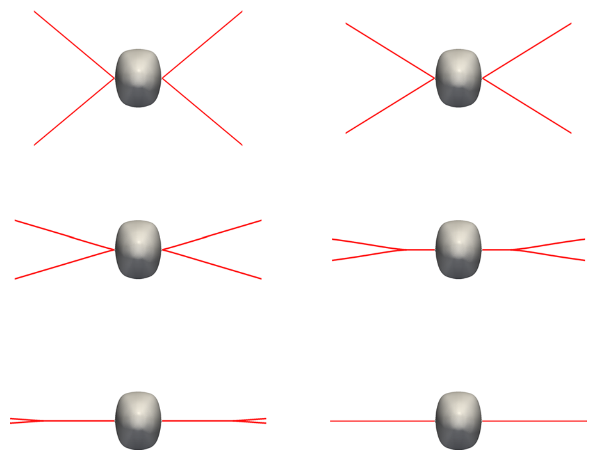

Fig. 3 Wing leading edges at the same instants as in Fig. 2

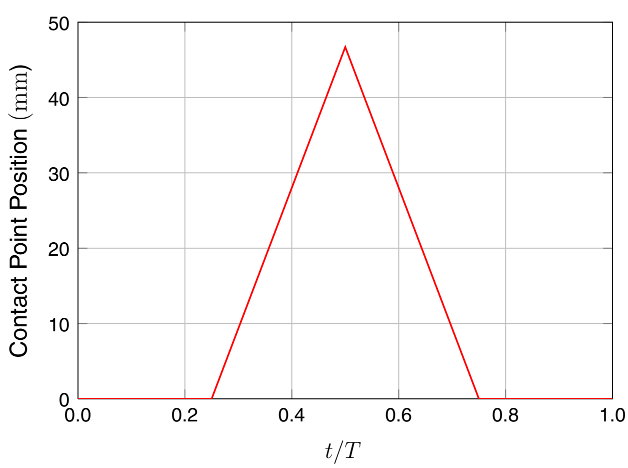

Fig. 4 Contact point position along the leading edge over a flapping cycle

position along the leading edge over a flapping cycle. The position is measured from the body.

The density and kinematic viscosity are $1.225\ \mathrm{kg/m^3}$ and $1.461 \times 10^{-5}\ \mathrm{m^2/s}$. The free-stream velocity is $4.5\ \mathrm{m/s}$. The Reynolds number based on average chord length and free-stream velocity is 5,423. Three cases are computed, with the angle of attack $\alpha = 0°, 5°$ and $10°$. The dimensions of the

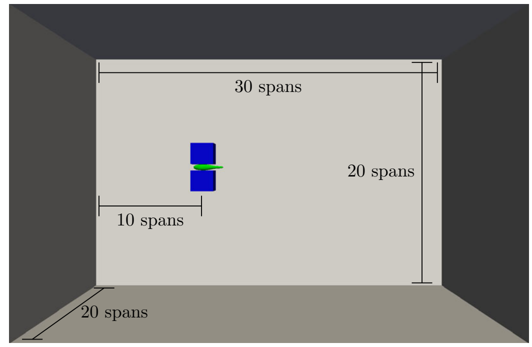

Fig. 5 Computational domain and mesh setup. Outer boundaries (*gray*), boundaries of the inner, structured meshes (*blue*), and body (*green*). (Color figure online)

Table 1 Number of nodes (*nn*) and elements (*ne*) in the meshes used

Surface mesh		
Single wing	*nn*	802
	ne	1,600
Body	*nn*	8,521
	ne	16,630
Volume mesh		
Inner	*nn*	405,002
	ne	2,303,920
Full ($\alpha = 0°$)	*nn*	1,143,613
	ne	6,844,706
Full ($\alpha = 5°$)	*nn*	1,227,618
	ne	7,353,540
Full ($\alpha = 10°$)	*nn*	1,152,367
	ne	6,896,762

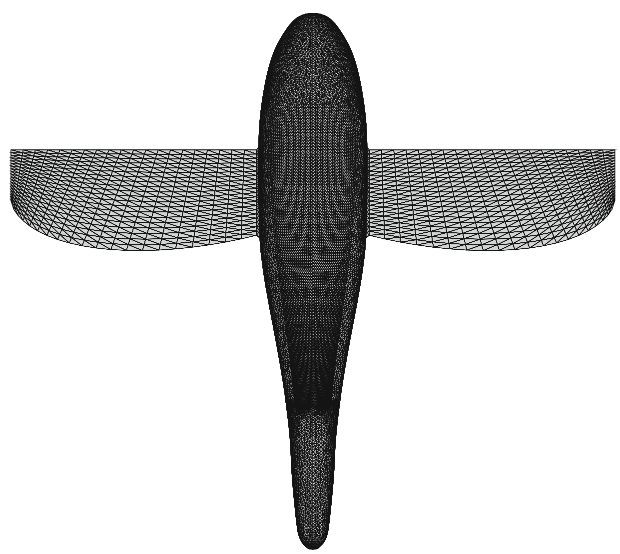

Fig. 6 Surface mesh at $t/T = 0.5$

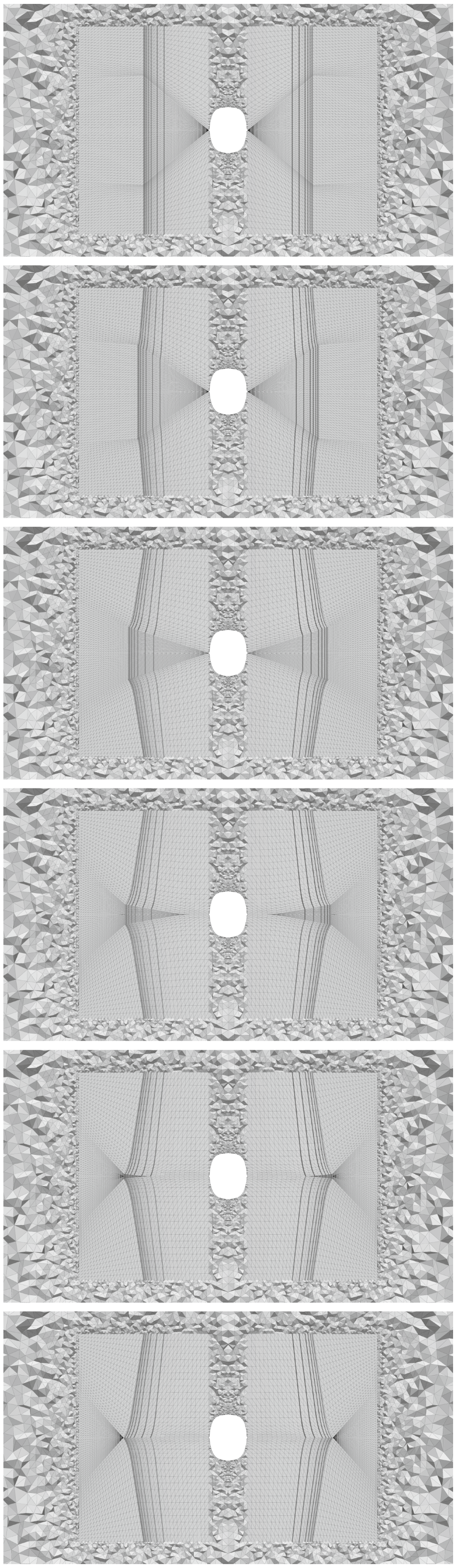

Fig. 7 Mesh (cut mid-chord) at the same instants as in Fig. 2

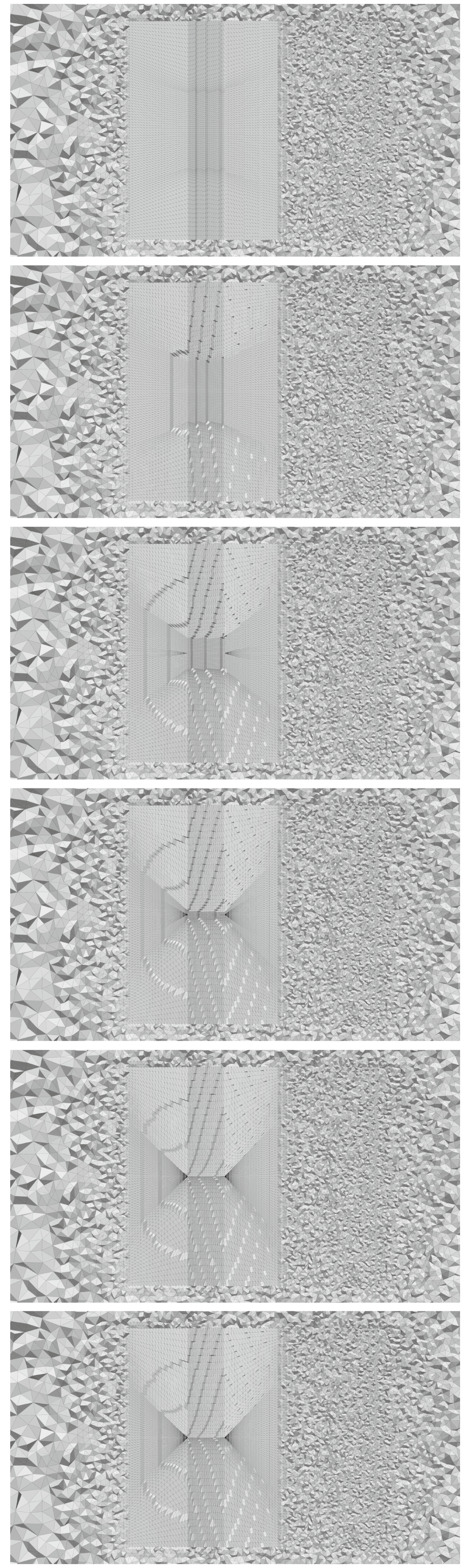

Fig. 8 Mesh (cut mid-span) at the same instants as in Fig. 2

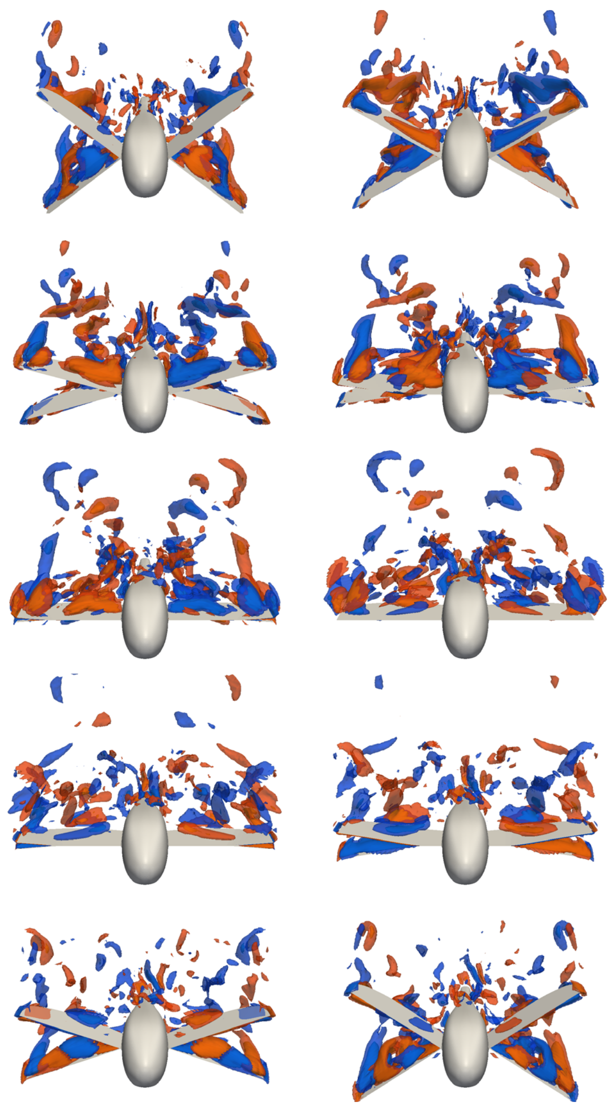

Fig. 9 Helicity isosurfaces (±5 and ±10 m^2/s^2) for α = 10° at t/T = 0.0, 0.1, 0.2, 0.3, 0.4, 0.5, 0.6, 0.7, 0.8 and 0.9 (*left* to *right* and then *top* to *bottom*). *Blue* is for negative values, and *red* for positive. (Color figure online)

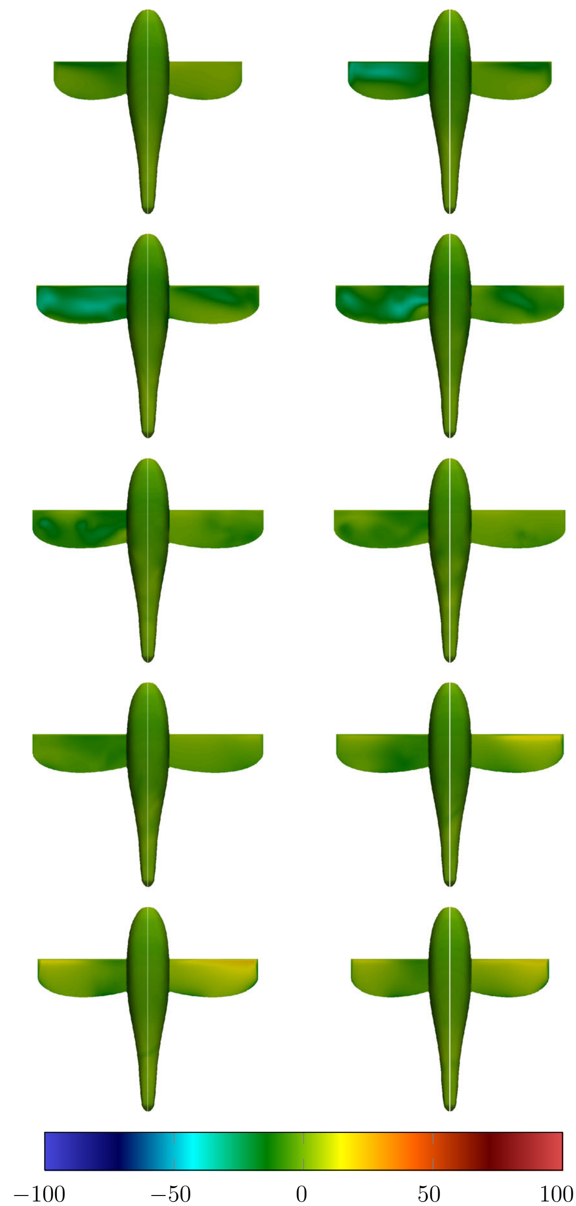

Fig. 10 Pressure (Pa) for $\alpha = 10°$ on the body and wing surfaces at the same instants as in Fig. 9. The upper surface of the upper wing (*left side*) and the lower surface of the lower wing (*right side*). (Color figure online)

computational domain, in spans of a single wing, are 30 × 20 × 20, and the distance between the inflow boundary and the leading edge is 10 (see Fig. 5). The boundary conditions are no-slip on the wings and body, uniform horizontal velocity at the inflow boundary, zero-stress at the outflow boundary, and slip at the upper, lower and side boundaries.

The meshes have structured, inner zones around the wings, and an unstructured, outer zone. Both the structured and unstructured zones are made of tetrahedral elements. Table 1 shows the number of nodes and elements in the meshes used. Figure 6 shows top view of the wing and body surface meshes. During the flapping motion, only the mesh in the inner zones move, and this is done with a special, algebraic mesh moving technique.

The structured, inner zones for each wing consist of four parts. Those parts each have 3 × 2 × 2 structured zones. Each zone has 20 × 20 × 20 hexahedral clusters made of 6 tetrahedral elements. Figures 7 and 8 show, for $\alpha = 0°$, the mesh at the same instants as in Fig. 2. The zones between the upper and lower wings collapse when the wings close, and the nodes in the neighboring zones also collapse accordingly. We note that a wing has split nodes except along its edges not attached to the body. However, when the wings are closed, the nodes on the upper surface of the upper wings and the lower surface of the lower wings become masters. When the

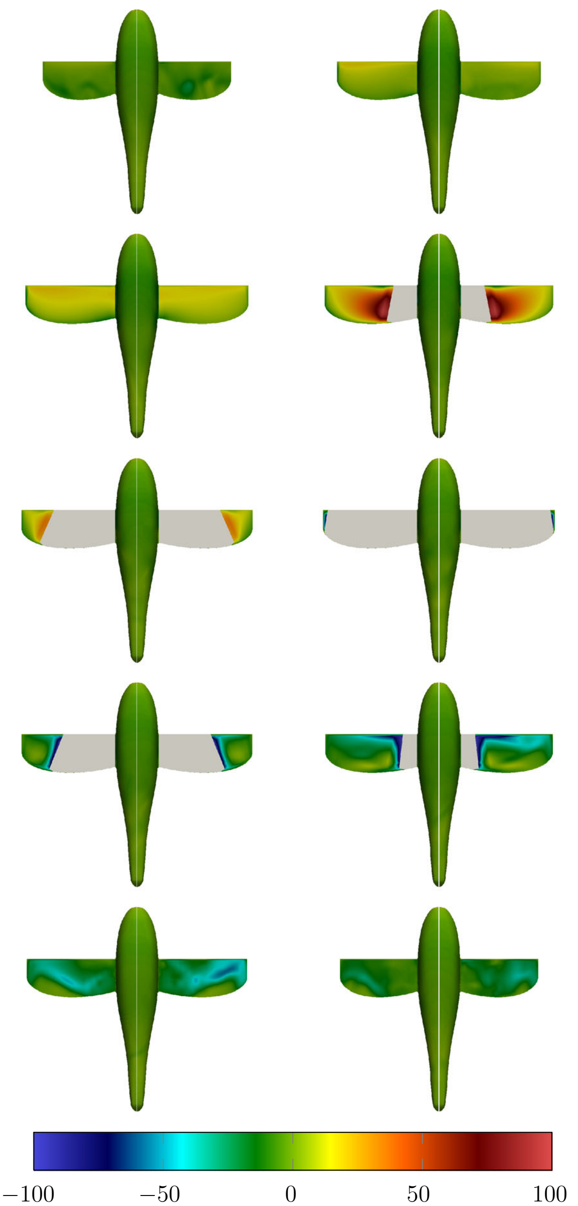

Fig. 11 Pressure (Pa) for $\alpha = 10°$ on the body and wing surfaces at the same instants as in Fig. 9. The lower surface of the upper wing (*left side*) and the upper surface of the lower wing (*right side*). The *white regions* are the closed parts of the wings. (Color figure online)

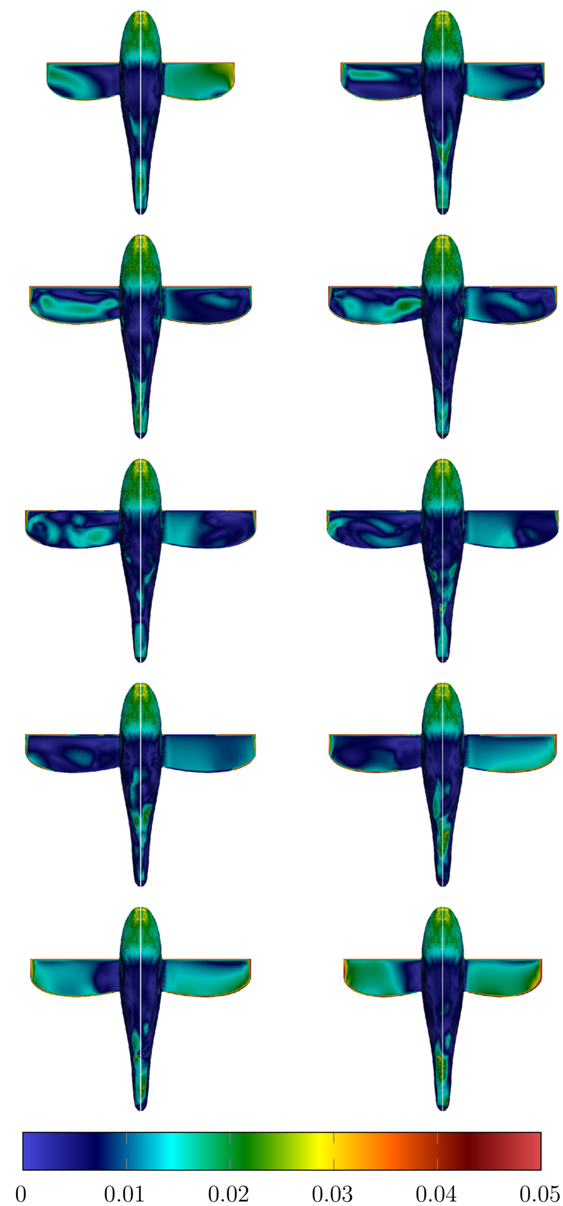

Fig. 12 Magnitude of the shear stress (Pa) for $\alpha = 10°$ on the body and the wing surfaces at the same instants as in Fig. 9. The upper surface of the upper wing (*left side*) and the lower surface of the lower wing (*right side*). (Color figure online)

wings are partially closed, at the contact point, the nodes on the lower surface of the upper wing are also masters while the nodes on the upper surface of the lower wings are slaves.

2.2 Computational conditions

We use the ST-SUPS and ST-VMS (convective form) methods for the first two and last two nonlinear iterations of each time step, essentially making the ST-VMS method the operative one. The ST-SUPS method is the original DSD/SST method. It was named "DSD/SST-SUPS" in [10] (i.e. the version with the SUPG/PSPG stabilization), and gained the shorter name "ST-SUPS" in [12]. The ST-VMS method [11] is the the variational multiscale version of the DSD/SST method, which was first called "DSD/SST-VMST" (i.e. the version with the VMS turbulence model) in [10]. The VMS components are from the residual-based VMS method given in [76–79]. In these methods, the stabilization parameter τ_{SUPS} comes from the τ_{SUPG} definition in [8], specifically the definition given by Eqs. (107)–(109) in [8], which can also be found as the definition given by Eqs. (7)–(9) in [9], with ν_{LSIC} from Eq. (17) in [9].

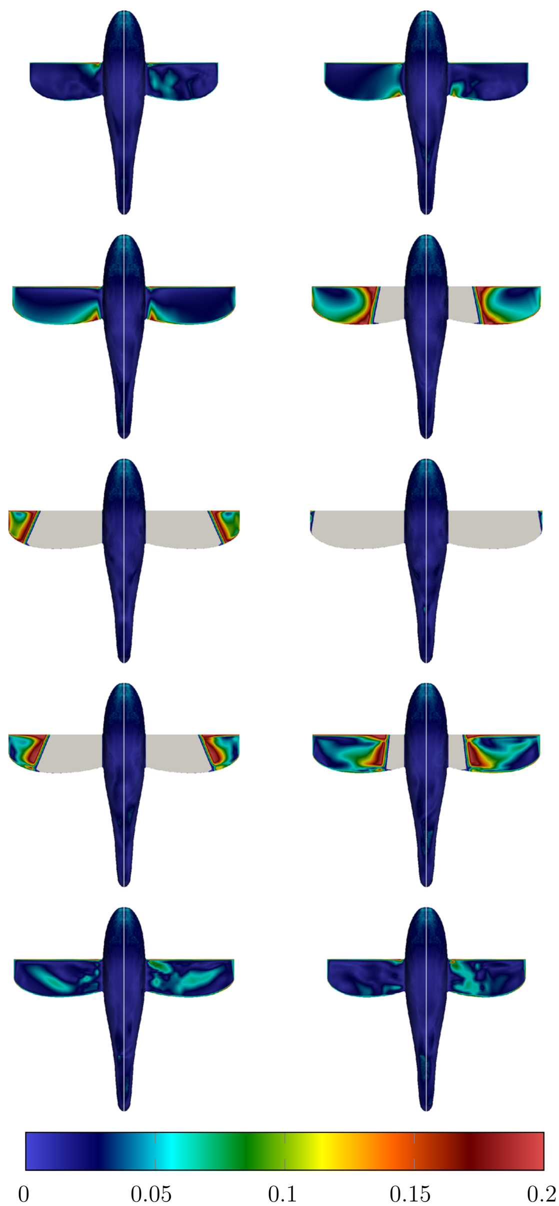

Fig. 13 Magnitude of the shear stress (Pa) for $\alpha = 10°$ on the body and the wing surfaces at the same instants as in Fig. 9. The lower surface of the upper wing (*left side*) and the upper surface of the lower wing (*right side*). The *white regions* are the closed parts of the wings. (Color figure online)

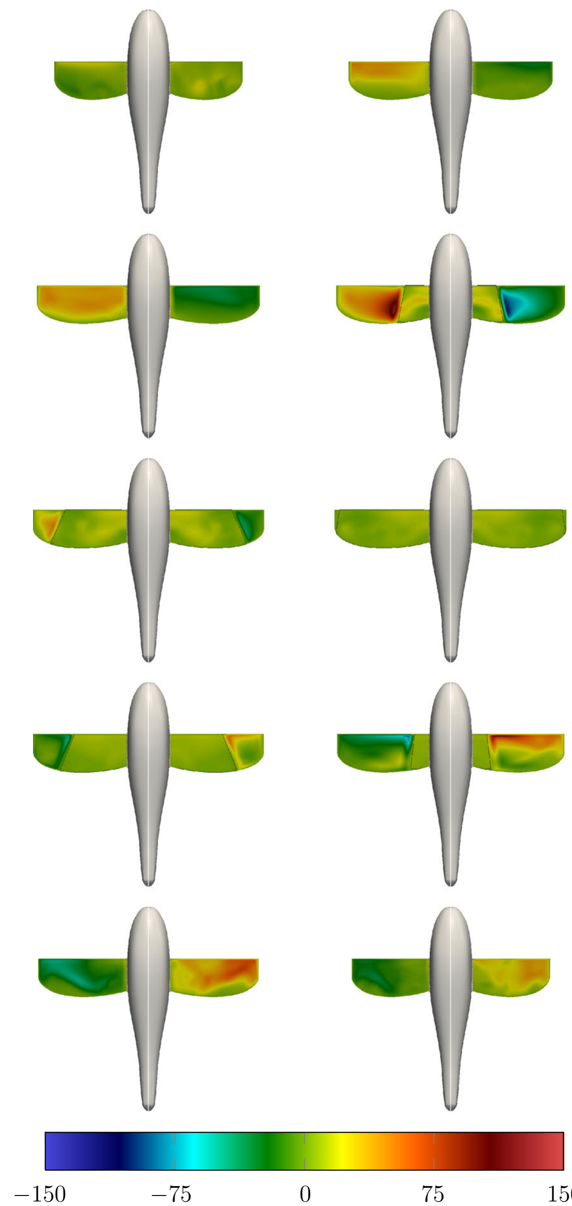

Fig. 14 Pressure difference (Pa) between the lower and upper surfaces for $\alpha = 10°$ at the same instants as in Fig. 9. The upper wing and closed wings (*left side*) and the lower wing and closed wings (*right side*). (Color figure online)

The time-step size is 4.51×10^{-4} s. At each angle of attack, prior to the flapping motion, we compute 550 time steps with the geometry at $t = 0$ to develop the flow field. For the first 500 time steps, only half of the computational domain is used, with slip boundary condition on the symmetry plane. The computed data is then copied to the other half of the mesh for the final 50 time steps of flow field development. The inflow velocity 4.5 m/s is reached by a sinusoidal ramping over the first 150 time steps, starting from 0.0 m/s. In computing the developed flow field, the number of GMRES iterations per nonlinear iteration is 150, 350, 450 and 800. In computing the flapping cycles, the number of GMRES iterations is 250, 500, 750 and 1,000. We compute three flapping cycles and display the results for the third cycle.

2.3 Results

We first present (in Figs. 9, 10, 11, 12, 13, 14), only for $\alpha = 10°$, results over (or in relationship to) the MAV body and wing surfaces. Figure 9 shows the helicity isosurfaces.

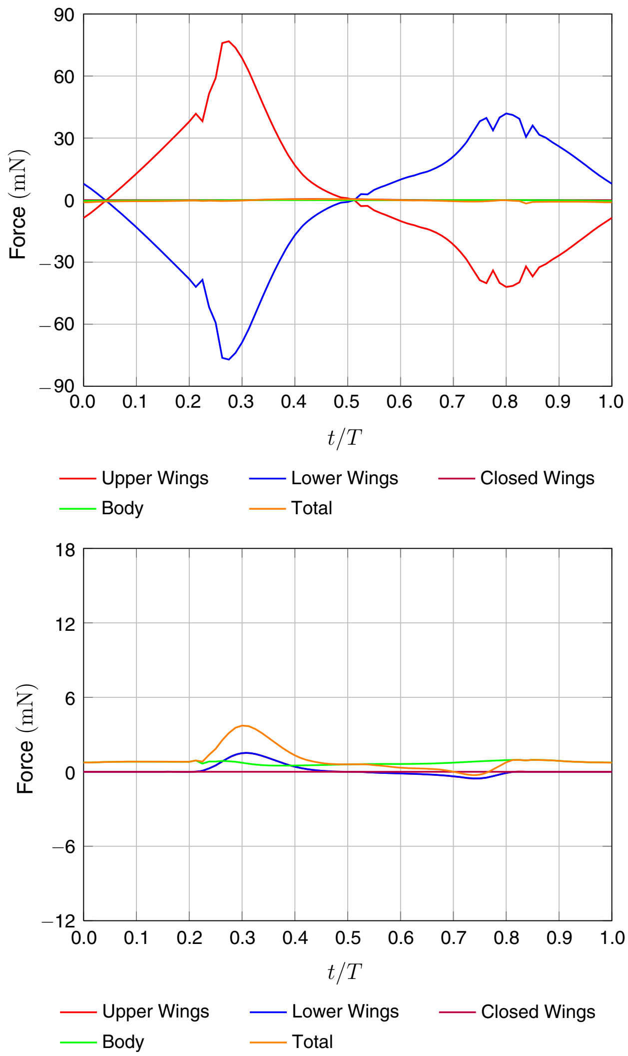

Fig. 15 Lift (*top*) and drag (*bottom*) for $\alpha = 0°$. (Color figure online)

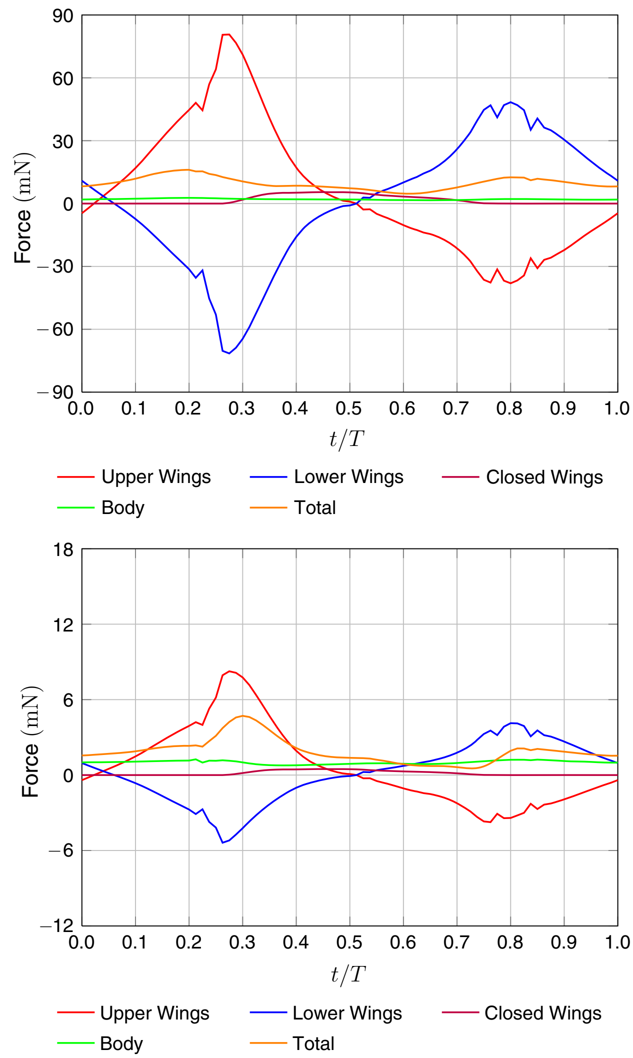

Fig. 16 Lift (*top*) and drag (*bottom*) for $\alpha = 5°$. (Color figure online)

The flow field near the wings is almost symmetric, but the flow behind the MAV is not. Figures 10 and 11 show pressure on the body and the wing surfaces. The pressure is almost symmetric, and therefore we use the left and right sides of the wing pictures for the upper and lower wings. For the body, however, both sides show the upper surface. Figures 12 and 13 show the magnitude of shear stress on the body and wing surfaces.Again, we use the left and right sides of the wing pictures for the upper and lower wings, and both sides of the body for the upper surface. Figure 14 shows the pressure difference between the upper and lower surfaces. The left sides of the wing pictures are for the upper wing, and the right sides for the lower wing. For the closed parts of the wings, both sides show the difference between the lower surface of the lower wing and the upper surface of the upper wing. Lift and drag are shown in Figs. 15, 16 and 17. We also show in those figures the contributions to the lift and drag from the upper and lower wings, the closed wings, and the body.

3 Concluding remarks

We have extended the ST-TC method to 3D computational analysis of flapping-wing aerodynamics of an MAV with wing clapping. The ST-TC method is a new version of the DSD/SST method, which is an interface-tracking (moving-mesh) method. The ST-TC method possess the desirable features of moving-mesh methods, including better resolution of the boundary layers, which is crucial in accurate computational analysis of flapping-wing aerodynamics. In its ST-TC version, the DSD/SST method is enhanced with a master–slave system that maintains the connectivity of the parent fluid mechanics mesh when there is contact between the moving interfaces. With that enhancement and because of its ST nature, the ST-TC method can deal with an actual contact between solid surfaces in flow problems with moving interfaces. It accomplishes that while still possessing the desirable features of moving-mesh methods, the key desir-

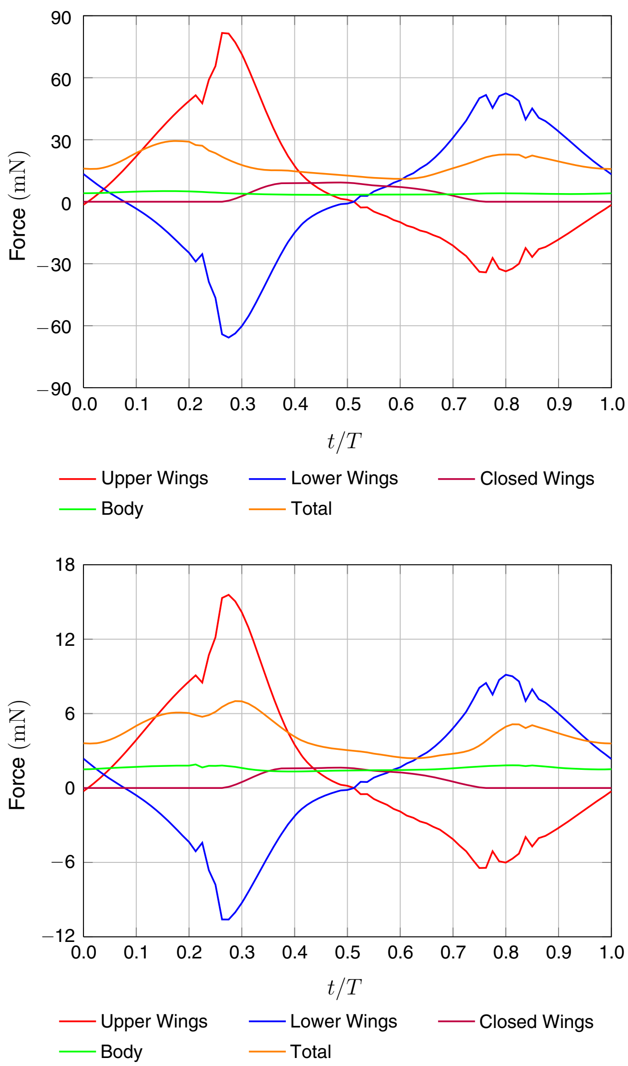

Fig. 17 Lift (*top*) and drag (*bottom*) for $\alpha = 10°$. (Color figure online)

able feature being better resolution of the boundary layers. Even before its ST-TC version, the DSD/SST method, with effective mesh update, was already able to handle moving-interface problems when the solid surfaces are in near contact or create near TC. Flapping-wing aerodynamics of an actual locust, with the forewings and hindwings crossing each other very close and creating near TC, is an example of successfully computed problems. Flapping-wing aerodynamics of an MAV with the wings of an actual locust is another example. In computational analysis of flapping-wing aerodynamics with wing clapping, however, we need to bring the wings into an actual contact when they clap. We showed here that with the ST-TC method we can do that. We used a model dragonfly MAV in the computational analysis, with the wings brought into an actual contact when they clap. The work presented shows that the ST-TC method has the accuracy of moving-mesh methods, flexibility of being able to deal with the TC in the fluid mechanics mesh when the wings are brought into contact, and the computational practicality of accomplishing these in 3D analysis.

Acknowledgments This work was supported in part by ARO Grant W911NF-12-1-0162 (second and third authors). It was also supported in part by Rice–Waseda research agreement (first author).

References

1. Weis-Fogh T (1973) Quick estimates of flight fitness in hovering animals, including novel mechanisms for lift production. J Exp Biol 59:169–230
2. Lighthill MJ (1973) On the Weis–Fogh mechanism of lift generation. J Fluid Mech 60:1–17
3. Kawamura Y, Souda S, Nishimoto S, Ellington CP (2008) Clapping-wing micro air vehicle of insect size. In: Kato N, Kamimura S (eds) Bio-mechanisms of swimming and flying, Chap. 26. Springer, Tokyo
4. Takizawa K, Tezduyar TE, Buscher A, Asada S (2014) Space-time interface-tracking with topology change (ST-TC). Comput Mech 54:955–971. doi:10.1007/s00466-013-0935-7
5. Tezduyar TE (1992) Stabilized finite element formulations for incompressible flow computations. Adv Appl Mech 28:1–44. doi:10.1016/S0065-2156(08)70153-4
6. Tezduyar TE, Behr M, Liou J (1992) A new strategy for finite element computations involving moving boundaries and interfaces—the deforming-spatial-domain/space-time procedure: I. The concept and the preliminary numerical tests. Comput Methods Appl Mech Eng 94:339–351. doi:10.1016/0045-7825(92)90059-S
7. Tezduyar TE, Behr M, Mittal S, Liou J (1992) A new strategy for finite element computations involving moving boundaries and interfaces—the deforming-spatial-domain/space-time procedure: II. Computation of free-surface flows, two-liquid flows, and flows with drifting cylinders. Comput Methods Appl Mech Eng 94:353–371. doi:10.1016/0045-7825(92)90060-W
8. Tezduyar TE (2003) Computation of moving boundaries and interfaces and stabilization parameters. Int J Numer Methods Fluids 43:555–575. doi:10.1002/fld.505
9. Tezduyar TE, Sathe S (2007) Modeling of fluid-structure interactions with the space-time finite elements: solution techniques. Int J Numer Methods Fluids 54:855–900. doi:10.1002/fld.1430
10. Takizawa K, Tezduyar TE (2011) Multiscale space-time fluid-structure interaction techniques. Comput Mech 48:247–267. doi:10.1007/s00466-011-0571-z
11. Takizawa K, Tezduyar TE (2012) Space-time fluid-structure interaction methods. Math Models Methods Appl Sci 22:1230001. doi:10.1142/S0218202512300013
12. Bazilevs Y, Takizawa K, Tezduyar TE (2013) Computational fluid-structure interaction: methods and applications. Wiley, Hoboken, ISBN 978-0470978771
13. Hughes TJR, Liu WK, Zimmermann TK (1981) Lagrangian–Eulerian finite element formulation for incompressible viscous flows. Comput Methods Appl Mech Eng 29:329–349
14. Ohayon R (2001) Reduced symmetric models for modal analysis of internal structural-acoustic and hydroelastic-sloshing systems. Comput Methods Appl Mech Eng 190:3009–3019
15. van Brummelen EH, de Borst R (2005) On the nonnormality of subiteration for a fluid-structure interaction problem. SIAM J Sci Comput 27:599–621
16. Bazilevs Y, Calo VM, Zhang Y, Hughes TJR (2006) Isogeometric fluid-structure interaction analysis with applications to arterial blood flow. Comput Mech 38:310–322

17. Khurram RA, Masud A (2006) A multiscale/stabilized formulation of the incompressible Navier–Stokes equations for moving boundary flows and fluid-structure interaction. Comput Mech 38:403–416
18. Bazilevs Y, Calo VM, Hughes TJR, Zhang Y (2008) Isogeometric fluid-structure interaction: theory, algorithms, and computations. Comput Mech 43:3–37
19. Dettmer WG, Peric D (2008) On the coupling between fluid flow and mesh motion in the modelling of fluid-structure interaction. Comput Mech 43:81–90
20. Bazilevs Y, Gohean JR, Hughes TJR, Moser RD, Zhang Y (2000) "Patient-specific isogeometric fluid-structure interaction analysis of thoracic aortic blood flow due to implantation of the Jarvik (2000) left ventricular assist device. Comput Methods Appl Mech Eng 198(2009):3534–3550
21. Bazilevs Y, Hsu M-C, Benson D, Sankaran S, Marsden A (2009) Computational fluid-structure interaction: methods and application to a total cavopulmonary connection. Comput Mech 45:77–89
22. Bazilevs Y, Hsu M-C, Zhang Y, Wang W, Liang X, Kvamsdal T, Brekken R, Isaksen J (2010) A fully-coupled fluid-structure interaction simulation of cerebral aneurysms. Comput Mech 46:3–16
23. Bazilevs Y, Hsu M-C, Zhang Y, Wang W, Kvamsdal T, Hentschel S, Isaksen J (2010) Computational fluid-structure interaction: methods and application to cerebral aneurysms. Biomech Model Mechanobiol 9:481–498
24. Bazilevs Y, Hsu M-C, Akkerman I, Wright S, Takizawa K, Henicke B, Spielman T, Tezduyar TE (2011) 3D simulation of wind turbine rotors at full scale. Part I: Geometry modeling and aerodynamics. Int J Numer Methods Fluids 65:207–235. doi:10.1002/fld.2400
25. Bazilevs Y, Hsu M-C, Kiendl J, Wüchner R, Bletzinger K-U (2011) 3D simulation of wind turbine rotors at full scale. Part II: fluid-structure interaction modeling with composite blades. Int J Numer Methods Fluids 65:236–253
26. Akkerman I, Bazilevs Y, Kees CE, Farthing MW (2011) Isogeometric analysis of free-surface flow. J Comput Phys 230:4137–4152
27. Hsu M-C, Bazilevs Y (2011) Blood vessel tissue prestress modeling for vascular fluid-structure interaction simulations. Finite Elem Anal Des 47:593–599
28. Nagaoka S, Nakabayashi Y, Yagawa G, Kim YJ (2011) Accurate fluid-structure interaction computations using elements without mid-side nodes. Comput Mech 48:269–276. doi:10.1007/s00466-011-0620-7
29. Bazilevs Y, Hsu M-C, Takizawa K, Tezduyar TE (2012) ALE-VMS and ST-VMS methods for computer modeling of wind-turbine rotor aerodynamics and fluid-structure interaction. Math Models Methods Appl Sci 22:1230002. doi:10.1142/S0218202512300025
30. Akkerman I, Bazilevs Y, Benson DJ, Farthing MW, Kees CE (2012) Free-surface flow and fluid-object interaction modeling with emphasis on ship hydrodynamics. J Appl Mech 79:010905
31. Bazilevs Y, Hsu M-C, Scott MA (2012) Isogeometric fluid-structure interaction analysis with emphasis on non-matching discretizations, and with application to wind turbines. Comput Methods Appl Mech Eng 249–252:28–41
32. Hsu M-C, Akkerman I, Bazilevs Y (2012) Wind turbine aerodynamics using ALE-VMS: Validation and role of weakly enforced boundary conditions. Comput Mech 50:499–511
33. Hsu M-C, Bazilevs Y (2012) Fluid-structure interaction modeling of wind turbines: simulating the full machine. Comput Mech 50:821–833
34. Akkerman I, Dunaway J, Kvandal J, Spinks J, Bazilevs Y (2012) Toward free-surface modeling of planing vessels: simulation of the Fridsma hull using ALE-VMS. Comput Mech 50:719–727
35. Minami S, Kawai H, Yoshimura S (2012) Parallel BDD-based monolithic approach for acoustic fluid-structure interaction. Comput Mech 50:707–718
36. Miras T, Schotte J-S, Ohayon R (2012) Energy approach for static and linearized dynamic studies of elastic structures containing incompressible liquids with capillarity: a theoretical formulation. Comput Mech 50:729–741
37. van Opstal TM, van Brummelen EH, de Borst R, Lewis MR (2012) A finite-element/boundary-element method for large-displacement fluid-structure interaction. Comput Mech 50:779–788
38. Yao JY, Liu GR, Narmoneva DA, Hinton RB, Zhang Z-Q (2012) Immersed smoothed finite element method for fluid-structure interaction simulation of aortic valves. Comput Mech 50:789–804
39. Larese A, Rossi R, Onate E, Idelsohn SR (2012) A coupled PFEM-Eulerian approach for the solution of porous FSI problems. Comput Mech 50:805–819
40. Bazilevs Y, Takizawa K, Tezduyar TE (2013) Challenges and directions in computational fluid-structure interaction. Math Models Methods Appl Sci 23:215–221. doi:10.1142/S0218202513400010
41. Bazilevs Y, Hsu M-C, Bement MT (2013) Adjoint-based control of fluid-structure interaction for computational steering applications. Procedia Comput Sci 18:1989–1998
42. Korobenko A, Hsu M-C, Akkerman I, Tippmann J, Bazilevs Y (2013) Structural mechanics modeling and FSI simulation of wind turbines. Math Models Methods Appl Sci 23:249–272
43. Korobenko A, Hsu M-C, Akkerman I, Bazilevs Y (2013) Aerodynamic simulation of vertical-axis wind turbines. J Appl Mech 81:021011. doi:10.1115/1.4024415
44. Bazilevs Y, Korobenko A, Deng X, Yan J, Kinzel M, Dabiri JO (2014) FSI modeling of vertical-axis wind turbines. J Appl Mech 81:081006. doi:10.1115/1.4027466
45. Yao JY, Liu GR, Qian D, Chen CL, Xu GX (2013) A moving-mesh gradient smoothing method for compressible CFD problems. Math Models Methods Appl Sci 23:273–305
46. Kamran K, Rossi R, Onate E, Idelsohn SR (2013) A compressible Lagrangian framework for modeling the fluid-structure interaction in the underwater implosion of an aluminum cylinder. Math Models Methods Appl Sci 23:339–367
47. Hsu M-C, Akkerman I, Bazilevs Y (2014) Finite element simulation of wind turbine aerodynamics: validation study using NREL Phase VI experiment. Wind Energy 17:461–481
48. Long CC, Marsden AL, Bazilevs Y (2013) Fluid-structure interaction simulation of pulsatile ventricular assist devices. Comput Mech 52:971–981. doi:10.1007/s00466-013-0858-3
49. Long CC, Esmaily-Moghadam M, Marsden AL, Bazilevs Y (2014) Computation of residence time in the simulation of pulsatile ventricular assist devices. Comput Mech 54:911–919. doi:10.1007/s00466-013-0931-y
50. Yao J, Liu GR (2014) A matrix-form GSM-CFD solver for incompressible fluids and its application to hemodynamics. Comput Mech 54:999–1012. doi:10.1007/s00466-014-0990-8
51. Long CC, Marsden AL, Bazilevs Y (2014) Shape optimization of pulsatile ventricular assist devices using FSI to minimize thrombotic risk. Comput Mech 54:921–932. doi:10.1007/s00466-013-0967-z
52. Hsu M-C, Kamensky D, Bazilevs Y, Sacks MS, Hughes TJR (2014) Fluid-structure interaction analysis of bioprosthetic heart valves: significance of arterial wall deformation. Comput Mech 54:1055–1071. doi:10.1007/s00466-014-1059-4
53. Takizawa K, Montes D, McIntyre S, Tezduyar TE (2013) Space-time VMS methods for modeling of incompressible flows at high Reynolds numbers. Math Models Methods Appl Sci 23:223–248. doi:10.1142/s0218202513400022
54. Takizawa K, Tezduyar TE (2012) Computational methods for parachute fluid-structure interactions. Arch Comput Methods Eng 19:125–169. doi:10.1007/s11831-012-9070-4
55. Takizawa K, Montes D, Fritze M, McIntyre S, Boben J, Tezduyar TE (2013) Methods for FSI modeling of spacecraft parachute

dynamics and cover separation. Math Models Methods Appl Sci 23:307–338. doi:10.1142/S0218202513400058
56. Takizawa K, Tezduyar TE, Boben J, Kostov N, Boswell C, Buscher A (2013) Fluid-structure interaction modeling of clusters of spacecraft parachutes with modified geometric porosity. Comput Mech 52:1351–1364. doi:10.1007/s00466-013-0880-5
57. Takizawa K, Tezduyar TE, Boswell C, Kolesar R, Montel K (2014) FSI modeling of the reefed stages and disreefing of the Orion spacecraft parachutes. Comput Mech 54:1203–1220. doi:10.1007/s00466-014-1052-y
58. Takizawa K, Tezduyar TE, Kolesar R, Boswell C, Kanai T, Montel K (2014) Multiscale methods for gore curvature calculations from FSI modeling of spacecraft parachutes. Comput Mech 54:1461–1476. doi:10.1007/s00466-014-1069-2
59. Takizawa K, Tezduyar TE, Boswell C, Tsutsui Y, Montel K (2014) Special methods for aerodynamic-moment calculations from parachute FSI modeling. Comput Mech. doi:10.1007/s00466-014-1074-5
60. Takizawa K, Bazilevs Y, Tezduyar TE, Hsu M-C, Øiseth O, Mathisen KM, Kostov N, McIntyre S (2014) Engineering analysis and design with ALE-VMS and space-time methods. Arch Comput Methods Eng 21:481–508. doi:10.1007/s11831-014-9113-0
61. Takizawa K, Schjodt K, Puntel A, Kostov N, Tezduyar TE (2013) Patient-specific computational analysis of the influence of a stent on the unsteady flow in cerebral aneurysms. Comput Mech 51:1061–1073. doi:10.1007/s00466-012-0790-y
62. Takizawa K, Takagi H, Tezduyar TE, Torii R (2014) Estimation of element-based zero-stress state for arterial FSI computations. Comput Mech 54:895–910. doi:10.1007/s00466-013-0919-7
63. Takizawa K, Bazilevs Y, Tezduyar TE, Long CC, Marsden AL, Schjodt K (2014) ST and ALE-VMS methods for patient-specific cardiovascular fluid mechanics modeling. Math Models Methods Appl Sci 24:2437–2486. doi:10.1142/S0218202514500250
64. Takizawa K (2014) Computational engineering analysis with the new-generation space-time methods. Comput Mech 54:193–211. doi:10.1007/s00466-014-0999-z
65. Suito H, Takizawa K, Huynh VQH, Sze D, Ueda T (2014) FSI analysis of the blood flow and geometrical characteristics in the thoracic aorta. Comput Mech 54:1035–1045. doi:10.1007/s00466-014-1017-1
66. Takizawa K, Tezduyar TE, Buscher A, Asada S (2014) Space-time fluid mechanics computation of heart valve models. Comput Mech 54:973–986. doi:10.1007/s00466-014-1046-9
67. Takizawa K, Torii R, Takagi H, Tezduyar TE, Xu XY (2014) Coronary arterial dynamics computation with medical-image-based time-dependent anatomical models and element-based zero-stress state estimates. Comput Mech 54:1047–1053. doi:10.1007/s00466-014-1049-6
68. Takizawa K, Henicke B, Puntel A, Kostov N, Tezduyar TE (2012) Space-time techniques for computational aerodynamics modeling of flapping wings of an actual locust. Comput Mech 50:743–760. doi:10.1007/s00466-012-0759-x
69. Takizawa K, Kostov N, Puntel A, Henicke B, Tezduyar TE (2012) Space-time computational analysis of bio-inspired flapping-wing aerodynamics of a micro aerial vehicle. Comput Mech 50:761–778. doi:10.1007/s00466-012-0758-y
70. Takizawa K, Tezduyar TE, Kostov N (2014) Sequentially-coupled space-time FSI analysis of bio-inspired flapping-wing aerodynamics of an MAV. Comput Mech 54:213–233. doi:10.1007/s00466-014-0980-x
71. Takizawa K, Tezduyar TE, McIntyre S, Kostov N, Kolesar R, Habluetzel C (2014) Space-time VMS computation of wind-turbine rotor and tower aerodynamics. Comput Mech 53:1–15. doi:10.1007/s00466-013-0888-x
72. Bazilevs Y, Takizawa K, Tezduyar TE, Hsu M-C, Kostov N, McIntyre S (May 2014) Aerodynamic and FSI analysis of wind turbines with the ALE-VMS and ST-VMS methods. Arch Comput Methods Eng 21:359–398. doi:10.1007/s11831-014-9119-7
73. Takizawa K, Tezduyar TE (2014) Space-time computation techniques with continuous representation in time (ST-C). Comput Mech 53:91–99. doi:10.1007/s00466-013-0895-y
74. Tezduyar TE, Takizawa K, Moorman C, Wright S, Christopher J (2010) Space-time finite element computation of complex fluid-structure interactions. Int J Numer Methods Fluids 64:1201–1218. doi:10.1002/fld.2221
75. Flytech wowwee dragonfly (September 2007) http://rcmania.com/reviews/flytech-dragonfly-wowwee/
76. Hughes TJR (1995) Multiscale phenomena: Green's functions, the Dirichlet-to-Neumann formulation, subgrid scale models, bubbles, and the origins of stabilized methods. Comput Methods Appl Mech Eng 127:387–401
77. Hughes TJR, Oberai AA, Mazzei L (2001) Large eddy simulation of turbulent channel flows by the variational multiscale method. Phys Fluids 13:1784–1799
78. Bazilevs Y, Calo VM, Cottrell JA, Hughes TJR, Reali A, Scovazzi G (2007) Variational multiscale residual-based turbulence modeling for large eddy simulation of incompressible flows. Comput Methods Appl Mech Eng 197:173–201
79. Bazilevs Y, Akkerman I (2010) Large eddy simulation of turbulent Taylor–Couette flow using isogeometric analysis and the residual-based variational multiscale method. J Comput Phys 229:3402–3414